RSC Advances

PAPER

Cite this: *RSC Adv.*, 2014, **4**, 44827

A multi-photoresponsive molecular-hybrid for dual-modal photoinactivation of cancer cells

Aurore Fraix,†[a] Stefano Guglielmo,†[b] Venera Cardile,[c] Adriana C. E. Graziano,[c] Ruxandra Gref,[d] Barbara Rolando,[b] Roberta Fruttero,*[b] Alberto Gasco[b] and Salvatore Sortino*[a]

Received 6th August 2014
Accepted 8th September 2014

DOI: 10.1039/c4ra08250h

www.rsc.org/advances

We report the design, synthesis, photochemical characterization and biological evaluation of a novel molecular conjugate in which two chromogenic centers, a porphyrin unit and a nitroaniline derivative, are covalently linked through an alkyl spacer. This molecular hybrid can be encapsulated in biocompatible, water soluble polymer nanoparticles where it shows satisfactory fluorescence emission and capability to generate simultaneously the cytotoxic singlet oxygen and nitric oxide upon excitation with visible light. The photoactive nanoassembly can be delivered to A375 melanoma cancer cells where it can be detected through its red fluorescence, and is capable of inducing amplified cell mortality by bimodal action due to the concomitant photoproduction of reactive oxygen and nitrogen oxygen species.

Introduction

Multimodal cancer therapies exploit either additive or synergistic effects arising from the generation of different active species for improving the therapeutic efficacy.[1] In this frame, the spatio-temporal control of the bio-active agents represents a challenging objective since it allows, in principle, maximization of the therapeutic action and minimization of side effects.[2] Light represents a powerful tool for the rapid introduction of active species in a biological environment, mimicking an "optical microsyringe" with exquisite control of three main factors such as site, timing and dosage, which are determining for the therapeutic outcome.[3–5] In addition, photochemical triggering offers the great benefit of not perturbing the physiological values of parameters such as temperature, pH and ionic strength, fundamental prerequisite for biomedical applications. These unique features make the photoactivated systems a powerful arsenal in the burgeoning field of nanomedicine with intriguing potential to tackle cancer diseases in a noninvasive way.[3–7]

Multidrug resistance (MDR), the major factor in the failure of many forms of chemotherapy,[8] calls for a shift of attention to alternative treatment modalities. At this regard, the light-controlled generation of reactive oxygen species (ROS) and reactive nitrogen oxygen species (RNOS) such as singlet oxygen ($^1O_2$) and nitric oxide (NO) by using appropriate photochemical precursors represents a fascinating and unconventional strategy.

$^1O_2$ is the key species in photodynamic therapy (PDT), a well-established therapeutic modality for the treatment of malignant lesions in humans. It implies the combined use of visible light, a non-toxic photosensitizing dye (PS) and the molecular oxygen.[9] The PS generally belongs to the class of porphyrins and phthalocyanines[10] and is administered by intravenous, intraperitoneal or topical route. It accumulates preferentially into the tumor cells as compared with the normal cells and its intracellular distribution is depending on its structure.[11] Illumination of the tumoral area with an opportune dose of appropriate wavelength light, leads to the population of the lowest and long-lived excited triplet state of the PS. The return of the system to the ground state occurs mainly by energy transfer to molecular oxygen, generating the highly reactive $^1O_2$ which induces selective tumor cell and tumor tissue destruction through a number of mechanisms.[12]

Nitric oxide (NO) is an important gaseous endogenous messenger which plays a variety of roles in the human physiology and pathophysiology.[13] NO contributes to maintain micro and macrovascular homeostasis inducing vasodilation, inhibition of platelet aggregation, modulation of platelet and leukocyte adherence to vessels, and inhibition of smooth muscle cell proliferation.[14] In the central nervous system it is implicated in neural signaling, neurotoxicity, neuroprotection, synaptic plasticity and modulation of behavioral pathways.[15] Peripherally NO modulates a number of reflexes by acting as neurotransmitter at the endings of non-adrenergic non-cholinergic

[a]*Laboratory of Photochemistry, Department of Drug Sciences, University of Catania, 95125 Catania, Italy. E-mail: ssortino@unict.it*

[b]*Department of Drug Science and Technology, University of Torino, 10125 Torino, Italy. E-mail: roberta.fruttero@unito.it*

[c]*Department of Bio-Medical Sciences, Physiology Division, University of Catania, 95125 Catania, Italy*

[d]*UMR CNRS 8612, Faculty of Pharmacy, Paris Sud University, 92290 Châtenay-Malabry, France*

† Contributed equally.

nerves.[15] NO is also one of the final effectors in the immune system, where it triggers tumoricidal, antimicrobial or anti-parasitic actions.[16] Indeed, NO plays important roles in the biology of tumors and in the inflammation processes.[17,18] Therefore, great attention has been paid to products able to release NO under physiological conditions as potential drugs to fight a variety of diseases.[19,20] NO-photodonors, namely molecules capable of producing NO under the action of the light, represent a particular class of these compounds.[21,22] They allow an accurate control of the timing, location and dosage of NO-release. This aspect is very important since NO can be therapeutic or toxic (double edged sword) depending on the doses.[23]

The combination of $^1O_2$ and NO represents a very appealing strategy in view of multimodal therapeutic systems. $^1O_2$ and NO share in fact several important features such as: (i) small size and absence of charge, (ii) capability to attack biological substrates of different nature (*i.e.*, lipids, proteins, and DNA), (iii) absence of multidrug resistance, (iv) confinement of their action to short distances from the production site inside the cells (<20 nm for $^1O_2$ and <200 μm for NO), due to their short lifetime, reducing systemic toxicity issues common to many conventional drugs. Besides, since NO photorelease is independent from O_2 availability, it very well complements PDT at the onset of hypoxic conditions, typical for some tumors, where PDT may fail.

The visualization of the phototherapeutic precursor in a cellular environment through fluorescence techniques represents an indispensable requisite in view of image-guided cancer phototherapy. This has recently led to the general term "photosensitizer fluorescence detection" in reference to all applications in which a PS is also used to generate fluorescence contrast.[24] Therefore, the creation of single platforms enabling simultaneous photogeneration of $^1O_2$ and NO and, at the same time, tracing in a cellular environment *via* fluorescence techniques is very challenging. We have recently reported a number of multifunctional nanoconstructs with imaging and bimodal therapeutic modalities by the non-covalent assembling of suitable PSs for PDT and tailored NO photodonors.[25] On these grounds, the achievement of molecular hybrids in which a PS for PDT and a NO photodonor are covalently connected without affecting the photochemical behaviour of the individual components, would represent a significant step forward with respect to the above non-covalent systems. These last can potentially suffer disassembling after penetration in the cellular environment and, as a consequence, photogenerate the cytotoxic agents in different sites of the cell compartment. On the other hand, molecular conjugates, would offer in principle the great advantage of a much more precise control of timing, location and dosage of the cytotoxic species. In fact, the covalent connection of the photoactive precursors ensures that the photodelivery events occur exactly in the "very same region of space" of the cell component. To this end, we have developed herein the novel multiphotoresponsive molecular hybrid **1** (Scheme 1) in which a porphyrin unit and a tailored NO photodonor are integrated within the same molecular skeleton through an alkyl spacer. In this contribution we report the synthesis, photochemical characterization and biological evaluation of this molecular conjugate and the related model compounds **2** and **3**. In particular, we show that the conjugate **1** (i) can be encapsulated within nanoparticles of the biocompatible and water soluble copolymer **4** used as suitable carrier system, (ii) photogenerates simultaneously $^1O_2$ and NO under visible light stimuli, (iii) exhibits satisfactory red fluorescence allowing the visualization of its localization in melanoma cancer cell, (iv) induces amplified cell mortality by bimodal photoaction (Scheme 1).

Results and discussion

Design and synthesis

In search of a viable strategy to construct a molecular hybrid able to display fluorescence properties associated to the simultaneous photogeneration of $^1O_2$ and NO we have deliberately chosen a nitroaniline derivative bearing a CF_3 substituent in the *ortho* position with respect to the nitro group and a tetrapyridyl porphyrin as suitable chromogenic units, respectively. We have demonstrated that such a class of nitroaniline-like chromophores are suitable NO photodonors as they satisfy several prerequisites for bio-applications including excitation with visible light and formation of non-toxic side photoproducts.[26,27] The twisted conformation adopted by the nitro group with respect to the aromatic plane is crucial for the NO photorelease. Similarly to other nitroaromatics having the same molecular conformation, the mechanism of NO release involves an initial nitro-to-nitrite photorearrangement followed by cleavage of the O–NO bond.[28] Besides, pyridyl porphyrins derivatives are good red photoemitters, excellent $^1O_2$ PS and, in addition, they can be *ad-hoc* derivatized *via* simple synthetic procedures.[29]

The rationale behind the choice of the above chromogenic components has its root in our previous works in which we have demonstrated that the non-covalent assembling of porphyrin centers and nitroaniline-based NO photodonors in a restricted region of space after incorporation in micelles,[30] nanoparticles[31] and host–guest complexes,[32] does not influence the photochemical behavior of both chromophores. Note that, in contrast to non-photoresponsive compounds, the preservation of the photobehavior of independent photoactive components after their covalent linking is not a "trivial result". In most cases, the response to light of the single photoactive units located in a so close proximity can be considerably influenced, in both nature and efficiency, by the occurrence of competitive photoprocesses (*i.e.*, photoinduced energy and/or electron transfer, non-radiative deactivation, *etc.*), which do not allow the individual components to work in parallel after light absorption. Taking into account these considerations, we have synthesized the conjugate **1** and the model compounds **2** and **3** according to the synthetic steps illustrated in Scheme 2. Reaction of **3c** and of 1-bromopropane with an excess of porphyrin **1a** in glacial acetic acid solution gave rise to the compounds **1** and **2** in poor yields, after flash chromatography purification. The products **3b** and **3** were easily obtained by treatment of the commercial 4-chloro-1-nitro-2-(trifluoromethyl)benzene (**3a**) with methylamine and *N*-methylpropylamine respectively, in absolute ethanol solution in

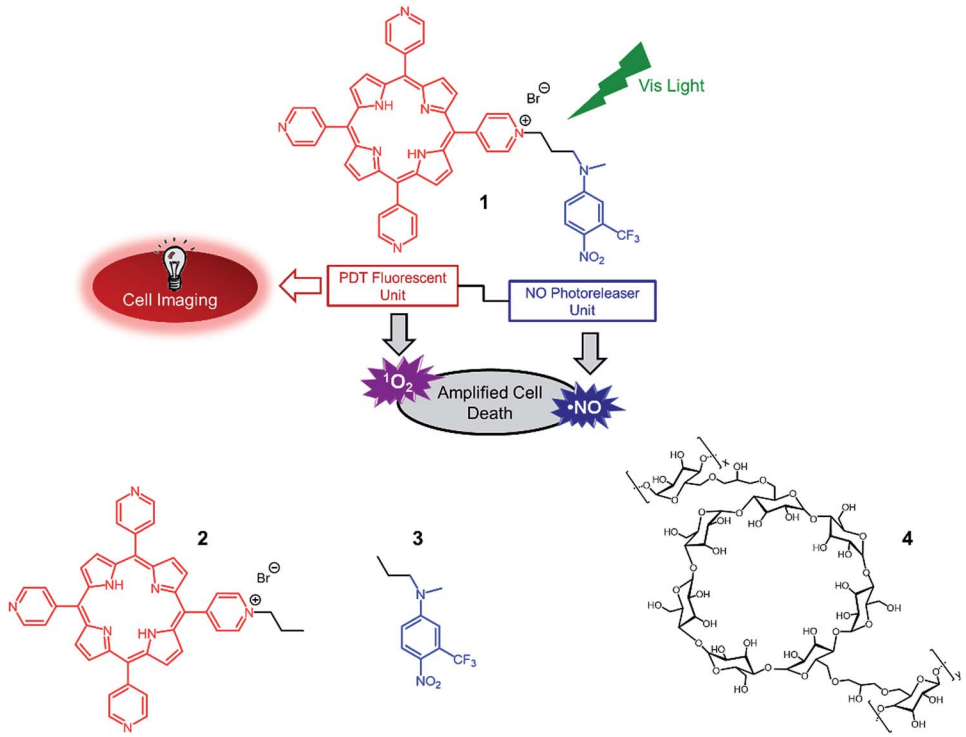

Scheme 1 Molecular structures of the conjugate **1**, the model compounds **2** and **3**, and the polymer carrier **4**.

the presence of Na_2CO_3. Intermediate **3c** was prepared by refluxing in acetonitrile 1,3-dibromopropane and **3b** in the presence of K_2CO_3.

Spectroscopic and photochemical properties

Fig. 1A shows the absorption and fluorescence emission spectra of the molecular hybrid **1** and the related model compounds in methanol solution. The absorption profile of **1** reflects fairly well that of an equimolar mixture of the model compounds **2** and **3**, with an experimental error of about 10%, accounting for only a weak interaction between the two chromophoric units in the ground state. Besides, **1** exhibits the typical dual band fluorescence emission of the porphyrin moiety, analogously to that observed for an optically matched solution of the model compound **2**. We obtained a fluorescence quantum yield $\Phi_f = 0.06$ for **1** and **2**, a value in the range reported for other pyridyl porphyrin derivatives.[33] This result suggests that the porphyrin core retains its emissive properties after the covalent linkage with the nitroaniline appendage.

Compound **1** is totally insoluble in both phosphate-buffered aqueous solution and in DMEM medium. However, compound **1** was slightly soluble in water containing 1% DMSO but unfortunately the presence of large aggregates precluded fluorescence. Focusing on solubility and aggregation issues in aqueous medium, cyclodextrin (CD) polymers offer the possibility of guest interaction with diverse binding sites, *i.e.* within the 3D macromolecular network and the CD cavities, thereby enhancing the apparent solubility and regulating the self-association tendency of drugs.[34] On these basis we used polymer **4** (see Scheme 1) as a suitable nanocarrier. Polymer **4** consists of β-CD units interconnected by epichlorohydrin spacers to form glyceryl cross-linked β-CD polymer. This polymer is well tolerated *in vivo*[35] and highly soluble in water where it exists under the form of nanoparticles (NPs) of *ca.* 25 nm in diameter.[36] Due to the presence of different hydrophobic nanodomains these NPs are able to entrap a variety of guests[34,37,38] with enhanced stability constants and payloads as compared with the unmodified β-CD.

Compound **1** becomes fairly soluble in the presence of aqueous dispersion of **4**. As shown in Fig. 1B, both the absorption and the emission profiles (spectra a and c) were very similar to those observed in methanol confirming the effective encapsulation of **1** within **4**, mainly under its monomeric form. The fluorescence quantum yield was even higher than in methanol solution, being $\Phi_f = 0.09$. Dynamic light scattering measurements indicate the average hydrodynamic diameters of *ca.* 35 nm for the NPs entrapping **1** (a, inset Fig. 1B). This value is slightly larger than that observed for the empty NPs (*ca.* 25 nm)[36] and in excellent agreement with that found for the same carrier entrapping chromophores of similar molecular sizes as **1**.[34,37,38] Interestingly, the absorption and emission characteristics (b and d in Fig. 1B) together with NPs sizes (b in the inset of Fig. 1B) were preserved quite well in DMEM medium where we obtained an emission quantum yield $\Phi_f = 0.07$ and a hydrodynamic diameter of *ca.* 33 nm.

The excited triplet state of the porphyrins is the key transient intermediate for the photosensitization of $^1O_2$ and its effective generation is thus crucial for the photodynamic action.[9] Laser flash photolysis with nanosecond time-resolution is a powerful

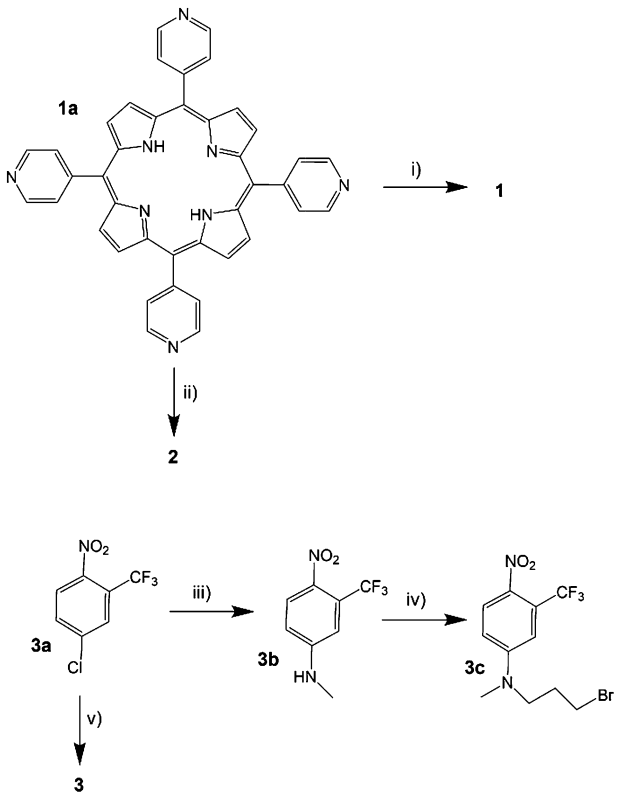

Scheme 2 Synthesis of the conjugate **1** and the model compounds **2** and **3**. Reagents and conditions: (i) **3c**, refluxing glacial CH_3COOH, 20 h; (ii) 1-bromopropane, glacial CH_3COOH, 120 °C (closed vessel), 20 h; (iii) CH_3NH_2 33% in absolute EtOH, Na_2CO_3, 70 °C, 36 h (closed vessel); (iv) 1,3-dibromopropane, K_2CO_3, refluxing CH_3CN, 5 days; (v) *N*-methylpropylamine, Na_2CO_3, absolute EtOH, 70 °C, 36 h (closed vessel).

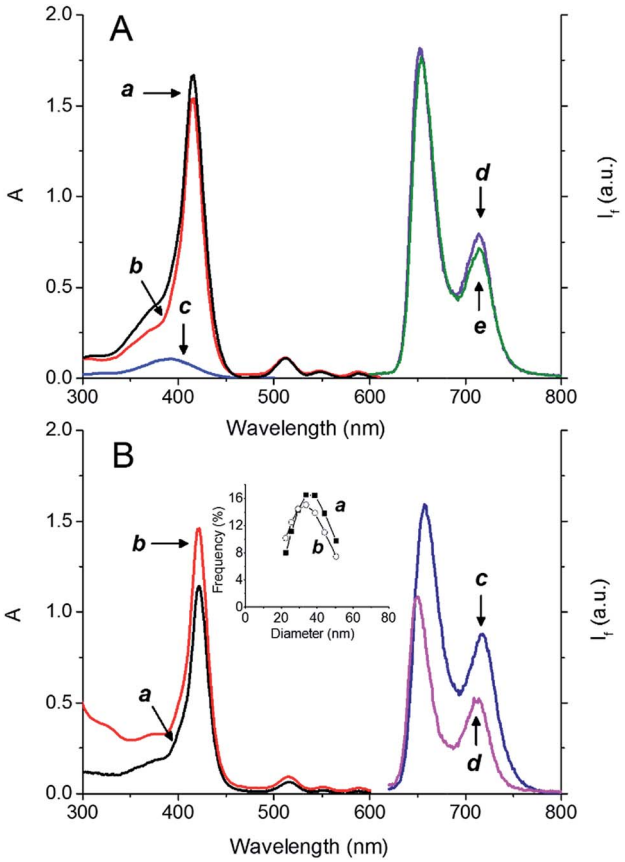

Fig. 1 (A) Absorption spectra of methanol solutions of **1** (a), **2** (b) and **3** (c). Fluorescence emission spectra (λ_{exc} = 505 nm) of methanol solutions of **1** (d) and **2** (e). [**1**] = [**2**] = [**3**] = 3.3 μM; T = 25 °C. (B) Absorption and fluorescence emission spectra of **1** in the presence of dispersions of **4** in aqueous phosphate buffer 10 mM pH 7.4 (a and c) and DMEM medium (b and d). The inset shows the hydrodynamic diameter for dispersions of **4** in the presence of **1** in aqueous phosphate buffer 10 mM pH 7.4 (a) and DMEM medium (b). [**1**] = 3.3 μM; [**4**] = 4 mg mL^{-1}; 25 °C.

tool for obtaining spectroscopic and kinetic features of excited triplets of porphyrins since these transient species exhibit very intense absorptions in the visible region and possess lifetimes falling in the microsecond time scale.[39] Fig. 2A shows that laser excitation of compound **1** in methanol results in the formation of a transient absorption with a maximum at *ca.* 450 nm and a bleaching due to the Soret ground-state absorption. This species which decays mono-exponentially with a lifetime of *ca.* 20 μs (inset Fig. 2A), is virtually the same to that obtained upon laser excitation of the model compound **2** (which decays with similar lifetime) and can be safely attributed to the lowest excited triplet state of the porphyrin core.[39]

Analogously to what observed for the fluorescence emission, the presence of the nitroaniline-derivative appendage does not influence the efficiency of the triplet population. In fact, since the two samples were optically matched at the excitation wavelength and the laser energy used was the same, the intensity of the transient absorption is directly related to the triplet quantum yield Φ_T. We obtained a value for Φ_T of 0.85 (see Experimental section), in excellent agreement with other tetrapyridyl porphyrin derivatives.[33]

The triplet state is also effectively populated when **1** is encapsulated in the NPs of the polymer carrier **4** in aqueous solution. Fig. 2B shows the transient absorption spectra obtained under these conditions and recorded at different delay times with respect to the initial laser pulse. Apart from a slight blue shift in the absorption maximum, the spectrum taken at the shortest delay time shows a profile very similar to that observed in methanol solution. The time evolution of the absorption reveals that no new transient species is formed concurrently to the triplet decay, ruling out any possible reaction of this species with the NPs. The excited triplet state decays mono-exponentially with a triplet lifetime of *ca.* 1000 μs (inset Fig. 2B), more than one order of magnitude longer than that observed in the organic solvent. The lengthening of the triplet decay observed is quite common upon incorporation of chromophores hosted in systems such as micelles, liposomes and CDs and is usually related to the protection exerted by the host cage against external quenching impurities, to a perturbation of the inter-system crossing process to the ground state, or to both.[40]

Energy transfer from the triplet of **1** to molecular oxygen results in the photogeneration of $^1O_2$. Time-resolved near-infrared

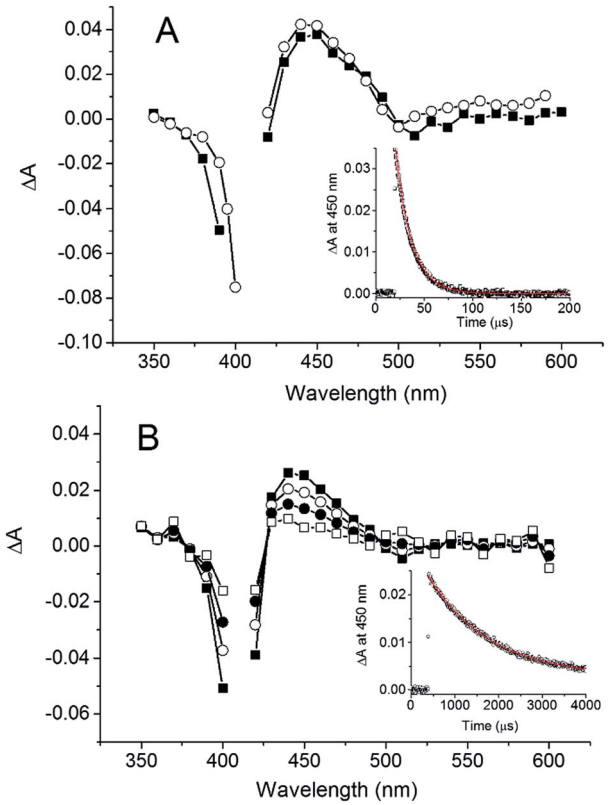

Fig. 2 (A) Transient absorption spectra observed 0.1 μs after 532 nm laser excitation ($E_{532} \sim 12$ mJ per pulse) of Ar-saturated and optically matched methanol solutions of **1** (■) and **2** (○). The inset shows the decay trace monitored at 450 nm and the related first-order fitting. (B) Transient absorption spectra observed 1 μs (■), 390 μs (○), 850 μs (●) and 1700 μs (□) after 532 nm laser excitation ($E_{532} \sim 12$ mJ per pulse) of Ar-saturated aqueous dispersions of **4** in phosphate buffer 10 mM pH 7.4 in the presence of **1**. The inset shows the decay trace monitored at 440 nm and the related first-order fitting. [**1**] = 3.3 μM; [**4**] = 4 mg mL^{-1}; 25 °C.

luminescence with sub-microsecond time resolution is the most suitable technique to unequivocally demonstrate the generation of singlet oxygen, $^1O_2$. This species, in fact, exhibits a typical luminescence signal at 1.27 μm with a lifetime ranging in the microseconds time-scale.[41] We have examined the singlet oxygen produced by energy transfer from **1** and the model compound **2** to molecular O_2, in partially deuterated (80% D_2O) aqueous dispersions of the carrier **4**. Fig. 3 shows the typical phosphorescence signal at 1270 nm observed for **1** and the model compound **2**. In both cases, the kinetic analysis of the decay traces gives a lifetime of *ca.* 40 μs, consistent with the reported value in the solvent used.[41]

Analogously to what observed for the precursor triplet state, the quantum yield of $^1O_2$ (Φ_Δ) for **1** was basically the same to that determined for the model **2**. We obtained a value for Φ_Δ = 0.55 (see Experimental) for both compounds, in excellent agreement to that reported for monocationic pyridyl porphyrins.[29]

The NO photorelease properties of the conjugate **1** are demonstrated by the direct and real-time monitoring of this

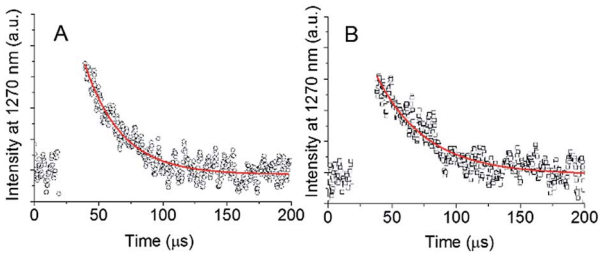

Fig. 3 Representative decay kinetic and related first-order fitting of $^1O_2$ observed upon 532 nm laser excitation ($E_{532} \sim 12$ mJ per pulse) of aqueous dispersion (80% D_2O) of **4** in the presence of either **1** (A) or the model compound **2** (B). [**1**] = [**2**] = 3.3 μM; [**4**] = 4 mg mL^{-1}; Phosphate buffer 10 mM, pH 7.4, 25 °C.

transient species using an ultrasensitive NO electrode which directly detects NO with nM concentration sensitivity by an amperometric technique.[42] The results illustrated in Fig. 4 provide evidence that the molecular hybrid **1** and the model compound **3** are stable in the dark but supply NO exclusively upon illumination with visible light. Note that, the rate for the NO photorelease was *ca.* 50 nM s^{-1} for both compounds suggesting that the porphyrin chromophore does not influence the capability of the NO photorelease in the conjugate.

Cell imaging and viability assay

The suitability of the multifunctional molecular conjugate **1** for cell fluorescence imaging and bimodal phototoxicity was demonstrated by *in vitro* experiments performed with A375 cells, a human amelanotic melanoma cell line. The cell uptake of **1** was determined after 4 h of incubation of a DMEM suspension of the carrier **4** in the presence of **1**, using fluorescence microscopy (Fig. 5). The typical porphyrin-associated

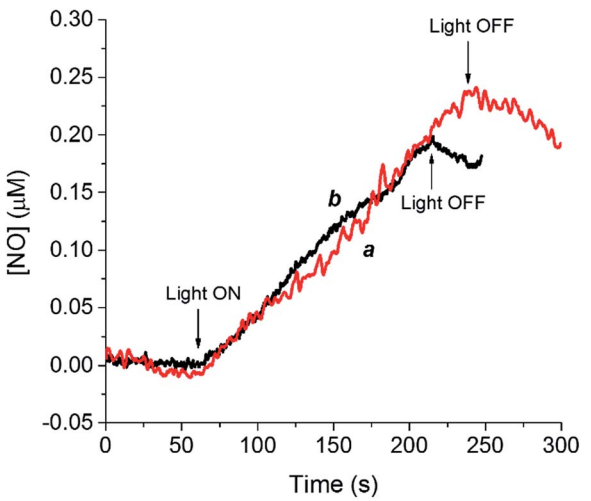

Fig. 4 NO release profiles observed upon irradiation (λ_{exc} = 405 nm) of aqueous dispersion of **4** in the presence of either **1** (a) or the model compound **3** (b). [**1**] = [**3**] = 3.3 μM; [**4**] = 4 mg mL^{-1}; phosphate buffer 10 mM, pH 7.4, 25 °C. The data are corrected for the different fraction of absorbed photons by **1** and the model compound **3**, at the excitation wavelength.

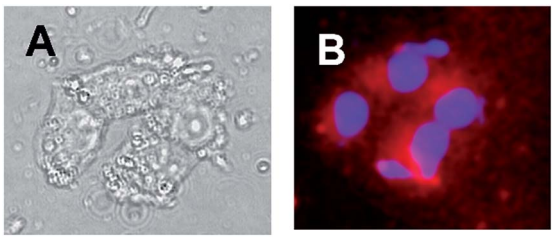

Fig. 5 Evaluation of the uptake of **1** by A375 melanoma cells. (A) Transmission microscopy. (B) Merging images of the cells analysed with a porphyrin and a DAPI emission filters, respectively, indicating accumulation of **1** in cells (red spots). [**1**] = 3.3 μM; [**4**] = 4 mg mL^{-1}; 25 °C.

fluorescence reveals that **1** is mainly accumulated in the cytoplasm of the melanoma cells, observed as red fluorescent spots, but no relevant nucleus associated fluorescence was observed. Fluorescence examination demonstrated the absence of obvious cell toxicity and of nuclear fragmentation, a marker of cell apoptosis, by DAPI staining.

To validate the feasibility of using this new molecular hybrid for bimodal phototherapeutic activity, the melanoma cells were incubated under different experimental conditions and were either kept in the dark or irradiated with visible light in the range 400–800 nm. Cell cytotoxicity was determined using the MTT assay 4 h after the completion of the irradiation. The results illustrated in Fig. 6 show that all samples displayed a low level of cytotoxicity in the dark, accounting for a good tolerance of the systems used. Besides, cells were not photosensitive in the absence of the photoactive compounds **1**, **2** or **3**. In contrast, considerable cell mortality was observed in the presence of these latter under illumination. In particular, the photoinduced mortality increased as a function of both the irradiation time

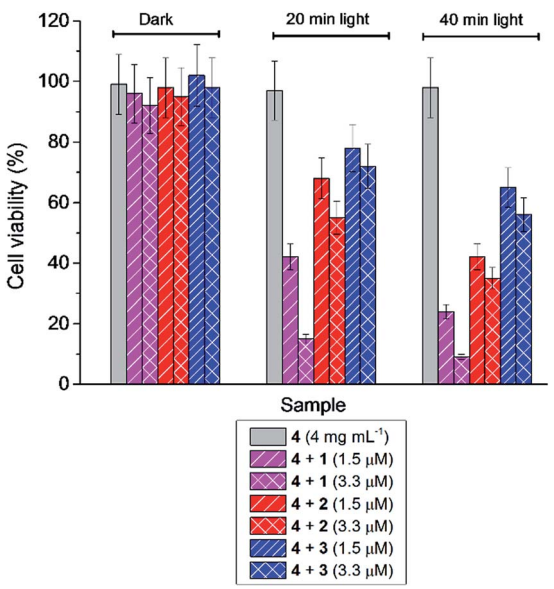

Fig. 6 Dark and photoinduced mortality (λ_{exc} 400–800 nm) of melanoma cells incubated with dispersion of **4** loaded with **1**, **2**, or **3**.

and the concentration of the photoactive components. In all cases, the level of photodynamic inactivation induced by the conjugate **1** was higher as compared to the value observed with the model compounds **2** and **3** under the same experimental conditions. This finding provides clear-cut evidence for the involvement of a bimodal photo-inactivation mechanism in neoplastic destruction, in which NO and $^1O_2$ are envisaged to play a key role. Note that, the amplified level of cell photomortality induced by the conjugate **1** is higher than that recently observed for the same cell lines in the case of a bichromophoric system in which the NO photodonor and the porphyrin centers were supramolecularly assembled in a ratio 1 : 1.[32] This is probably due to the photodelivery of both ROS and RNOS in the "very same region of space" of the cell compartment, as result of the covalent connection between the two photoprecursors in the conjugate **1**.

Conclusions

We have developed herein a novel photoactivable molecular hybrid combining three-in-one photofunctionalities. The two chromogenic units of the conjugate "ignore" each other in the excited state, as proven by the excellent preservation of their photophysical and photochemical properties, and thus can be operated independently under the exclusive control of visible light inputs. Specifically, the porphryrin core exhibits satisfactory red fluorescence and excellent photosensitization of $^1O_2$, while the nitroaniline acts as a NO photodispenser. Remarkably, this conjugate (i) can be delivered by polymer NPs in cancer cells, where it can be easily mapped by fluorescence microscopy and (ii) induces amplified level of cell mortality by bimodal action most likely due to a combined effect of the simultaneous photogeneration of ROS and RNOS in the same region of space. To our knowledge, this represents the first example of molecular hybrid exhibiting the convergence of dual therapeutic photoaction and imaging capability in a single molecular structure and opens fascinating possibilities for further studies on image-guided multimodal therapy in *in vivo* model systems.

Experimental section

Synthesis

All reagents were of the highest commercial grade available and were used without further purification. All solvents used (from Sigma-Aldrich) were analytical grade. Compounds **1a** and **3a** were purchased from Sigma-Aldrich. ^1H and ^{13}C NMR spectra were recorded on a Bruker Avance 300 at 300 and 75 MHz respectively, using $SiMe_4$ as internal standard. Low resolution mass spectra were recorded with a Finnigan-Mat TSQ-700. High resolution mass spectra were recorded on a Bruker BioApex Fourier transform ion cyclotron resonance (FT-ICR) mass spectrometer equipped with an Apollo I ESI source, a 4.7 T superconducting magnet, and a cylindrical infinity cell (Bruker Daltonics, Billerica, MA, USA). Melting points were determined with a capillary apparatus (Büchi 540). Flash column chromatography was performed on silica gel (Merck Kieselgel 60,

230–400 mesh ASTM), or on neutral aluminum oxide (Fluka Aluminum Oxide for Chromatography, 0.05–0.15 mm, Brockmann activity I). The progress of the reactions was monitored by thin layer chromatography (TLC) on 5 cm × 20 cm plates with a layer thickness of 0.2 mm. Organic solvents were removed under vacuum at 30 °C. Elemental analyses (C, H, N) of the target compounds **1** and **3** were performed by REDOX Snc Monza, and the results are within 0.4% of the theoretical values. The purity of compound **2** (>97%) was assessed by HPLC. Analyses were performed on an Acquity Ultra Performance LC™, Waters Corporation Milford MA, USA, equipped with BSM, SM, CM and PDA detector. The analytical column was a Phenomenex Synergi 4 μ, Max-RP, 150 × 2 mm. Compound was dissolved in CH_3OH. The mobile phase consisted of CH_3OH/water with 0.1% formic acid 50/50. HPLC retention time (t_R) was obtained at flow rates of 0.3 mL min^{-1}, and the column effluent was monitored at 236 and 420 nm.

***N*-Methyl-4-nitro-3-(trifluoromethyl)aniline (3b).** In a closed vessel **3a** (5 g, 22 mmol), 33% solution of CH_3NH_2 in absolute EtOH (10 eq.) and Na_2CO_3 (10 eq.) in 100 mL of absolute EtOH were stirred under heating at 70 °C for 36 hours. The mixture was allowed to reach room temperature, and then concentrated under reduced pressure. The residue was taken up with CH_2Cl_2, washed with water and brine, dried over Na_2SO_4 and concentrated under reduced pressure. The crude product was purified by flash chromatography on silica gel, eluent 40% CH_2Cl_2/PE, to afford the title product as a yellow solid (87%); mp (CCl_4) 114–115 °C. ^{1}H-NMR ($CDCl_3$): δ 2.96 (3H, d, J = 5.1 Hz, CH_3), 4.89 (1H, br signal, NH), 3.11 (3H, s, CH_3N), 6.66 (1H, dd, J_1 = 9.0 Hz, J_2 = 2.4 Hz aromatic), 6.93 (1H, d, J = 2.4 Hz, aromatic), 8.05 (1H, d, J = 9.0 Hz, aromatic). ^{13}C-NMR ($CDCl_3$): δ 30.1, 110.87 (q, J = 6.75 Hz), 112.2, 122.3 (q, J = 271 Hz), 126.6 (q, J = 33 Hz), 129.2, 136.2, 152.8. MS CI (isobutane) (m/z): 221 [MH^+].

***N*-(3-Bromopropyl)-*N*-methyl-4-nitro-3-(trifluoromethyl)aniline (3c).** In a 500 mL round bottom flask a mixture of **3b** (3.3 g 15 mmol), 1,3-dibromopropane (10 eq.) and K_2CO_3 (3 eq.) was refluxed in 300 mL of CH_3CN for 5 days. The mixture was allowed to reach room temperature and concentrated under reduced pressure. The residue was taken up with CH_2Cl_2, washed with water and brine, dried over Na_2SO_4 and concentrated under reduced pressure. The crude product was purified by flash chromatography on silica gel, eluent 30% CH_2Cl_2/PE, to afford the title product as a yellow solid (30%); mp ($MeOH/H_2O$) 66.7–67.3 °C. ^{1}H-NMR ($CDCl_3$): δ 2,19 (2H, quintuplet, J = 6 Hz, $CH_2CH_2CH_2$), 3.15 (3H, s, CH_3), 3.46 (2H, t, J = 6 Hz, CH_2N), 3.67 (2H, t, J = 6 Hz, CH_2Br), 6.78 (1H, m, aromatic), 7.00 (1H, s, aromatic), 8.05 (1H, m, aromatic). ^{13}C-NMR ($CDCl_3$): δ 29.5, 30.3, 39.0, 50.6, 109.8 (q, J = 6.75 Hz), 112.3, 122.4 (q, J = 272 Hz), 126.5 (q, J = 32 Hz), 130.0, 135.6, 151.8. MS CI (isobutane) (m/z): 341/343 [MH^+].

***N*-Methyl-4-nitro-*N*-propyl-3-(trifluoromethyl)aniline (3).** In a closed vessel **3a** (1 g, 4.4 mmol), *N*-methylpropylamine (10 eq.) and Na_2CO_3(10 eq.) in 40 mL of absolute EtOH were stirred under heating at 70 °C for 36 hours. The mixture was allowed to reach room temperature and concentrated under reduced pressure. The residue was taken up with CH_2Cl_2, washed with water and brine, dried over Na_2SO_4 and concentrated under reduced pressure. The crude product was purified by flash chromatography on silica gel, eluent 40% CH_2Cl_2/PE, to afford the title product as a yellow solid (70%); mp (H_2O): 79.6–80.9 °C. ^{1}H-NMR ($CDCl_3$): δ 0.97 (3H, t, J = 7.5 Hz, $CH_2CH_2CH_3$), 1.67 (2H, sextet, J = 7.5 Hz, $CH_2CH_2CH_3$), 3.11 (3H, s, CH_3N), 3.42 (2H, t, J = 7.5 Hz, CH_2N), 6.70 (1H, dd, J_1 = 9.3 Hz, J_2 = 2.7 Hz aromatic), 6.93 (1H, d, J = 2.7 Hz, aromatic), 8.05 (1H, d, J = 9.3 Hz, aromatic). ^{13}C-NMR ($CDCl_3$): δ 11.3, 20.1, 38.9, 54.3, 109.60 (q, J = 6.6 Hz), 112.0, 122.5 (q, J = 272 Hz), 126.48 (q, J = 33 Hz), 129.1, 131.3, 152.0. MS CI (isobutane) (m/z): 263 [MH^+]. Anal. C, H, N.

1-(3-{Methyl[4-nitro-3-(trifluoromethyl)phenyl]amino}propyl)-4-(10,15,20-tripyridin-4-ylporphyrin-5-yl)pyridinium bromide (1). In a 100 mL round bottom flask, **1a** (0.5 g, 0.81 mmol) and **3c** (0.5 eq.) were dissolved in 20 mL of glacial acetic acid and refluxed for 20 hours. The mixture was allowed to reach room temperature, and concentrated under reduced pressure. The residue was taken up with boiling methanol and filtered. The filtrate was concentrated under reduced pressure. The crude compound was purified by flash chromatography on neutral alumina, eluent 3–5% CH_3OH/CH_2Cl_2, to afford the title product as a dark red solid (16%); mp > 300 °C. ^{1}H-NMR (D_6-DMSO): δ −3.05 (2H, s, 2 NH, pyrroles), 2.61 (2H, quint, J = 7.5 Hz, CH_2-CH_2CH_2), 3.30 (3H, s, CH_3N), 3.93 (2H, t, J = 7.5 Hz, CH_2N), 5.07(2H, t, J = 7.5 Hz, CH_2N^+pyr), 7.21 (1H, s, aromatic), 7.24 (1H, d, J = 9 Hz aromatic), 8.20 (1H, d, J = 9 Hz, aromatic), 8.28 (6H, d, J = 6 Hz, aromatic), 8.94–9.11 (16H, m, aromatic), 9.59 (2H, d, J = 6 Hz, aromatic). HR-MS expected for $C_{51}H_{38}F_3N_{10}O_2$ 879.3125; found 879.3137. Anal. C, H, N.

1-Propyl-4-(10,15,20-tripyridin-4-ylporphyrin-5-yl)pyridinium bromide (2). The product was obtained starting from **1a** and 1-bromopropane with the procedure used for the preparation of **1**. The crude compound was purified on neutral alumina column, eluent 3–5% CH_3OH/CH_2Cl_2, to give the expected product as a dark red solid (21%); mp > 300 °C, HPLC t_R: 7.6 min. ^{1}H-NMR (D_6-DMSO): δ −3.03 (2H, s, 2 NH, pyrroles), 1.21 (3H, t, J = 7.5 Hz), 2.31 (2H, sext, J = 7.5 Hz, $CH_2CH_2CH_3$), 4.93 (2H, t, J = 7.5 Hz, CH_2N^+), 8.30 (6H, d, J = 6 Hz, aromatic), 8.96–9.13 (16H, m, aromatic), 9.57 (2H, d, J = 6 Hz, aromatic). HR-MS expected for $C_{43}H_{33}N_8$ 661.2822; found 661.2820.

The β-CD polymer **4** was prepared by crosslinking β-CD with epichlorohydrin, under strong alkaline conditions, following a previously described method.[36]

Sample preparation

Solution of **4** was prepared by stirring overnight 4 mg mL^{-1} of **4** in either aqueous phosphate buffer 10 mM at pH 7.4 or DMEM medium. Compounds **1**, **2** and **3** were dissolved in methanol and slowly evaporated to form a thin film. These films were then hydrated with solutions of **1**. The mixtures were stirred for 5 hours at 40 °C and then the final solutions were left to equilibrate at room temperature and filtered.

Instrumentation

Steady-state absorption, emission, and NPs sizes. UV/Vis absorption and fluorescence spectra were recorded with a

thermostated HP-8452 diode array spectrophotometer and Fluorolog-2 (Model, F-111) spectrofluorimeter respectively. All measurements were performed in a thermostated quartz cell (1 cm path length, 3 mL capacity). NPs sizes were measured by a dynamic light scattering Horiba LS 550 apparatus equipped with a diode laser with a wavelength of 650 nm.

Fluorescence images were acquired using a Leica DMRB fluorescence microscope (Leica Microsystems Srl, Milan, Italy) equipped with a computer-assisted Nikon digital camera (Nital SpA, Turin, Italy).

Laser flash photolysis. All of the samples were excited with the second harmonic of Nd-YAG Continuum Surelite II-10 laser (532 nm, 6 ns FWHM), using quartz cells with a path length of 1.0 cm. The excited solutions were analyzed with a Luzchem Research mLFP-111 apparatus with an orthogonal pump/probe configuration. The probe source was a ceramic xenon lamp coupled to quartz fiber-optic cables. The laser pulse and the mLFP-111 system were synchronized by a Tektronix TDS 3032 digitizer, operating in pre-trigger mode. The signals from a compact Hamamatsu photomultiplier were initially captured by the digitizer and then transferred to a personal computer, controlled by Luzchem Research software operating in the National Instruments LabView 5.1 environment. The solutions were deoxygenated by bubbling with a vigorous and constant flux of pure argon (previously saturated with solvent). In all of these experiments, the solutions were renewed after each laser shot (in a flow cell of 1 cm optical path), to prevent probable auto-oxidation processes. The sample temperature was 295 ± 2 K. The energy of the laser pulse was measured at each shot with a SPHD25 Scientech pyroelectric meter.

Singlet oxygen detection. Photogeneration of $^1O_2$ upon laser excitation of the photosensitizer was monitored by luminescence measurements in oxygen-saturated solutions. The near-IR luminescence of singlet oxygen at 1.27 μm results from the forbidden transition $^3\Sigma_g^- \leftarrow {}^1\Delta_g$; this was probed orthogonally to the exciting beam with a pre-amplified (low impedance) Ge-photodiode (Hamamatsu EI-P, 300 ns resolution) maintained at −196 °C and coupled to a long-pass silicon filter (>1.1 μm) and an interference filter (1.27 μm). Pure signal of $^1O_2$ were obtained as difference between signals in air- and Ar-saturated solutions. The temporal profile of the luminescence was fitted to a single-exponential decay function with the exclusion of the initial portion of the plot, which was affected by scattered excitation light, fluorescence, and the formation profile of singlet oxygen itself.

Nitric oxide detection. NO release was measured with a World Precision Instrument, ISO–NO meter, equipped with a data acquisition system, and based on direct amperometric detection of NO with short response time (<5 s) and sensitivity range 1 nM–20 μM. The analog signal was digitalized with a four-channel recording system and transferred to a computer. The sensor was accurately calibrated by mixing standard solutions of $NaNO_2$ with 0.1 M H_2SO_4 and 0.1 M KI according to the reaction:

$$4H^+ + 2I^- + 2NO_2^- \rightarrow 2H_2O + 2NO + I_2$$

Irradiation was performed in a thermostated quartz cell (1 cm path length, 3 mL capacity, 25 °C) by using a 200 mW continuum laser with $\lambda_{exc} = 405$ nm. NO measurements were carried out under stirring with the electrode positioned outside the light path in order to avoid NO signal artefacts due to photoelectric interference on the ISO–NO electrode.

Determination of fluorescence, triplet and $^1O_2$ quantum yields

Fluorescence quantum yields were determined by using optically matched solution at the excitation wavelength of compounds **1** and **2** and aqueous solution of *para*-tetrakis-(-methylpyridiniumyl)porphyrin as a standard ($\Phi_f = 0.047$)[33] through the following equation:

$$\Phi_f = \Phi_{f(s)}(In^2/I_{(s)}n^2_{(s)})$$

where $\Phi_{f(s)}$ is the fluorescence quantum yield of the standard; I and $I_{(s)}$ are the areas of the fluorescence spectra of the compounds and the standard, respectively; n and $n_{(s)}$ are the refraction index of the solvents used for the compounds and the standard. In any case the absorbance at the excitation wavelength was less than 0.1.

Quantum yields for the triplet formation were determined by using optically matched solution at the excitation wavelength of compounds **1** and **2** and aqueous solution of the same standard as above ($\Phi_T = 0.92$).[33] The top ΔA of the triplet signal from each sample was plotted as a function of the laser intensity. In this case the initial part of each set of data points is proportional to the product $\Phi_T \times \varepsilon_{T-T}$, where Φ_T and ε_{T-T} are the quantum yield of the triplet state and its molar absorption coefficient, respectively. By taking into account that all solutions are almost optically matched at the excitation wavelength and that large changes in the ε_{T-T} are fairly unlikely, being substantially unchanged the band profiles, Φ_T values may be directly estimated by the different slopes (π) of the straight-lines obtained from the linear portion of the plots, *via* the simple equation;

$$\Phi_T = \Phi_{T(s)}\pi/\pi_{(s)}$$

$^1O_2$ quantum yield were determined by using optically matched solution at the excitation wavelength of compounds **1** and **2** and 5,10,15,20-tetrakis(4-sulfonatophenyl)-21*H*,23*H*-porphyrin in D_2O as a standard ($\Phi_\Delta = 0.6$).[43] The luminescence of the $^1O_2$ was recorded at different intensity of the laser pulse and the luminescence at initial time (L_Δ at $t = 0$) was extrapolated from the curve fitting. The values of L_Δ at $t = 0$, were then plotted against the laser intensity, and the related slopes (χ) were compared. The values of Φ_Δ were determined by using the following equation:

$$\Phi_\Delta = \Phi_{\Delta(s)}\chi/\chi_{(s)}$$

where $\chi_{(s)}$ and χ are the slopes of the plots of the $^1O_2$ luminescence, determined at initial time against the energy of the laser pulse for the standard and the compounds, respectively.

Experiments with cells

American Type Culture Collection (Rockville, MD, USA) was maintained in Dulbecco's modified Eagle's medium (DMEM) containing 10% fetal calf serum (FCS), 2.0 mM L-glutamine, 100 U/mL penicillin, 100 μg mL^{-1} streptomycin, and 25 μg mL^{-1} fungizone (Sigma-Aldrich, Italy), and incubated at 37 °C in humidified atmosphere containing 5% CO_2. Cells from confluent cultures were detached using trypsin/EDTA and seeded in complete DMEM medium. For cell staining, the cells were cultured in 12-well culture dishes for 24 hours. The medium was removed and replaced with medium without phenol red containing the solution of the sample for 4 hours. The cells were first washed with PBS, then fixed with 4% formaldehyde. After washing with PBS cells were incubated with 4,6-diamino-2-phenylindole (DAPI) (1 : 10 000; Invitrogen) for 10 min.

The photocytotoxicity experiments were carried out by irradiating the cells incubated either without or with the photoactive components with a 150 W Xe lamp through a cut-off filter at 400 nm. Cell proliferation was assessed by MTT assays, based on the conversion of a substrate containing a tetrazolium ring to spectrophotometrically detectable formazan by mitochondrial dehydrogenases. Briefly, cells were seeded at an initial density of 8×10^3 cells per microwell in flat-bottomed 200 μL microplates, incubated at 37 °C in a humidified atmosphere containing 5% CO_2 for 24 hours. Subsequently, part of the cells were maintained as media controls while others were incubated with the photoactive compounds. In both cases complete DMEM without phenol red was used. Next, 20 μL of 0.5% 3-(4,5-dimethyl-thiazol-2-yl)2,5-diphenyl-tetrazolium bromide in PBS were added to each microwell. Following 4 h of incubation at 37 °C, the supernatant was removed and replaced with 100 μL of DMSO. The optical density of each well sample was measured with a microplate spectrophotometer reader (Digital and Analog Systems, Rome, Italy) at 550 nm. The cell viability (%) was calculated according to the following equation:

$$\text{Cell viability (\%)} = [A_{\text{Before}} - (A_{\text{After}}/A_{\text{Before}})] \times 100$$

where, A_{Before} and A_{After} are the absorbance values of the wells treated with samples before and after irradiation respectively. Each experiment was repeated at least three times in triplicate and the mean ± SEM for each value was calculated. Statistical analysis of results [Student's *t* test for paired and unpaired data; variance analysis (ANOVA)] was performed using the statistical software package SYSTAT, version 11 (Systat Inc., Evanston IL, USA). A difference was considered significant at $p < 0.05$.

Acknowledgements

We thank AIRC, Project IG-12834, for financial support to the AIRC fellow AF and funding of the research. Financial support from MIUR (PRIN 2011) and from the Marie Curie Program # 608407 CYCLON-HIT (FP7-PEOPLE-ITN-2013) is also acknowledged.

Notes and references

1 N. L. Komarova and C. R. Boland, *Nature*, 2013, **499**, 291.
2 D. Lane, *Nat. Biotechnol.*, 2006, **24**, 163.
3 S. Sortino, *J. Mater. Chem.*, 2012, **22**, 301.
4 C. Brieke, F. Rohrbach, A. Gottschalk, G. Mayer and A. Heckel, *Angew. Chem., Int. Ed.*, 2012, **51**, 8446.
5 Q. Shao and B. Xing, *Chem. Soc. Rev.*, 2010, **39**, 2835.
6 B. Jang, J.-Y. Park, C.-H. Tung, I.-H. Kim and Y. Choi, *ACS Nano*, 2011, **5**, 1086.
7 N. Stephanopoulos, G. J. Tong, S. C. Hsiao and M. B. Francis, *ACS Nano*, 2010, **4**, 6014.
8 G. Szakács, J. K. Paterson, J. A. Ludwig, C. Booth-Gent and M. M. Gottesman, *Nat. Rev. Drug Discovery*, 2006, **3**, 219.
9 R. K. Pandey and G. Zheng, in *The Porphyrin Handbook*, ed. K. M. Smith, K. Kadish and R. Guilard, Academic Press, San Diego, 2000, vol. 6, pp. 157–230.
10 A. B. Ormond and H. S. Freeman, *Materials*, 2013, **6**, 817.
11 A. P. Castano, T. N. Demidova and M. R. Hamblin, *Photodiagn. Photodyn. Ther.*, 2004, **1**, 279.
12 A. P. Castano, T. N. Demidova and M. R. Hamblin, *Photodiagn. Photodyn. Ther.*, 2005, **2**, 91.
13 *Nitric Oxide: Biology and Pathobiology*, ed. L. J. Ignarro, Elsevier Inc., 2010.
14 R. C. Jin and J. Loscalzo, *J. Blood Med.*, 2010, **1**, 147.
15 J. V. Esplugues, *Br. J. Pharmacol.*, 2002, **135**, 1079.
16 J. E. Albina and J. S. Reichner, *Cancer Metastasis Rev.*, 1998, **17**, 39.
17 D. Fukumura, S. Kashiwagi and R. K. Jain, *Nat. Rev. Cancer*, 2006, **6**, 521.
18 J. L. Wallace, *Mem. Inst. Oswaldo Cruz*, 2005, **100**, 5.
19 P. G. Wang, M. Xian, X. Tang, X. Wu, Z. Wen, T. Cai and A. J. Janczuk, *Chem. Rev.*, 2002, **102**, 1091.
20 *Nitric oxide donors*, ed. P. G. Wang, T. B. Cai and N. Taniguchi, Wiley-VCH, Weinheim, 2005.
21 S. Sortino, *Chem. Soc. Rev.*, 2010, **39**, 2903.
22 P. C. Ford, *Nitric Oxide*, 2013, **34**, 56.
23 Q. Jia, A. J. Janczuk, T. Cai, M. Xian, Z. Wen and P. G. Wang, *Expert Opin. Ther. Pat.*, 2002, **12**, 819.
24 J. P. Celli, B. Q. Spring, I. Rizvi, C. L. Evans, K. S. Samkoe, S. Verma, B. W. Pogue and T. Hasan, *Chem. Rev.*, 2010, **12**, 2795.
25 A. Fraix, N. Kandoth and S. Sortino, in *Specialist Periodical Reports in Photochemistry*, 2013, vol. 41, p. 302.
26 E. B. Caruso, S. Petralia, S. Conoci, S. Giuffrida and S. Sortino, *J. Am. Chem. Soc.*, 2007, **129**, 480.
27 S. Conoci, S. Petralia and S. Sortino, EP2051935A1/US20090191284, 2006.
28 K. Fukuhara, M. Kurihara and N. Miyata, *J. Am. Chem. Soc.*, 2001, **123**, 8662.
29 D. K. Deda, C. Pavani, E. Caritá, M. S. Baptista, H. E. Toma and K. Araki, *J. Porphyrins Phthalocyanines*, 2012, **16**, 56.
30 E. B. Caruso, E. Cicciarella and S. Sortino, *Chem. Commun.*, 2007, 5028.
31 N. Kandoth, E. Vittorino, M. T. Sciortino, I. Colao, A. Mazzaglia and S. Sortino, *Chem.–Eur. J.*, 2012, **18**, 1684.
32 A. Fraix, R. A. Gonçalves, V. Cardile, A. C. E. Graziano, T. A. Theodossiou, K. Yannakopoulou and S. Sortino, *Chem.–Asian J.*, 2013, **8**, 2634.
33 K. Kalyanasundaram, *Inorg. Chem.*, 1984, **23**, 2453.

34 N. Kandoth, V. Kirejev, S. Monti, R. Gref, M. B. Ericson and S. Sortino, *Biomacromolecules*, 2014, **15**, 1768.
35 S. Daoud-Mahammed, J. L. Grossiord, T. Bergua, C. Amiel, P. Couvreur and R. Gref, *J. Biomed. Mater. Res., Part A*, 2008, **86**, 736.
36 M. Othman, K. Bouchemal, P. Couvreur, D. Desmaële, E. Morvan, T. Pouget and R. Gref, *J. Colloid Interface Sci.*, 2011, **354**, 517.
37 A. Fraix, N. Kandoth, I. Manet, V. Cardile, A. C. E. Graziano, R. Gref and S. Sortino, *Chem. Commun.*, 2013, **49**, 4459.
38 E. Deniz, N. Kandoth, A. Fraix, V. Cardile, A. C. E. Graziano, D. Lo Furno, R. Gref, F. M. Raymo and S. Sortino, *Chem.–Eur. J.*, 2012, **18**, 15782.
39 M. Montalti, A. Credi, L. Prodi and M. T. Gandolfi, *Handbook of Photochemistry*, CRC Press, Boca Raton, 3rd edn, 2006.
40 S. Monti and S. Sortino, *Chem. Soc. Rev.*, 2002, **31**, 287.
41 F. Wilkinson, W. P. Helman and A. B. Ross, *J. Phys. Chem. Ref. Data*, 1993, **22**, 113.
42 P. N. Coneski and M. H. Schoenfisch, *Chem. Soc. Rev.*, 2012, **41**, 3753.
43 J. Mosinger and Z. Micka, *J. Photochem. Photobiol., A*, 1997, **107**, 77.